Adjustment of Tall Buildings Behavior by Guided Optimization of Magnetorheological-Dampers Control Parameters

Amin Akhnoukh *, Ahmed Farid , Ahmed Hasan , Youssef Rashed

Posted Date: 28 February 2023

doi: 10.20944/preprints202302.0518.v1

Keywords: MR-dampers, structural control, MR-fluids, seismic excitation, smart buildings

Article

Adjustment of Tall Buildings Behavior by Guided Optimization of Magnetorheological-Dampers Control Parameters

Amin Akhnoukh [1*], Ahmed Fady Farid[2], Ahmed M.M. Hassan[2,3], and Youssef F. Rashed[2]

[1] Construction Management Department, East Carolina University, Greenville, North Carolina
[2] Civil Engineering Department; Cairo University, Cairo, Egypt
[3] CIEM, School of Engineering and Applied Science, Nile University, Egypt
* Correspondence: akhnoukha17@ecu.edu ; Tel.: (001 501 249 7961, AA)

Abstract: Magneto-rheological dampers (MR-dampers) are increasingly used in construction applications to reduce the dynamic response of structures to seismic activities or severe wind loading. Sensors attached to the structure will signal the computer to supply the dampers with electric charge that transfers the MR fluid to a near-solid material with different physical and mechanical properties (viscoelastic behavior). Control algorithms govern the fluid to near-solid conversion, which controls the behavior of the damper, and the performance of the structure under the seismic or wind loading event. The successful optimization of control parameters minimize the overall structural response to dynamic forces. The main objective of this research is to change the output behavior of specific floors within a building subjected to seismic excitation by optimizing the MR-dampers control parameters to impact the behavior of a specific floor or number of floors within the building. The adjustment of control parameters to attain this objective was validated in multiple case studies throughout this research. The successful implementation of the research outcome will result in optimized MR-damper design to meet the performance-based criteria of building projects.

Keywords: MR-dampers, structural control, MR-fluids, seismic excitation, smart buildings

1. Introduction

Building structures and bridges are vulnerable to shocks due to seismic loading. In recent years, major earthquake events resulted in the death of thousands and billions of dollars of asset losses. Solutions to mitigate earthquake losses included the development of performance-based design codes, the use of high-performance construction materials with improved durability and long-term performance [1-5] and self-healing materials. One of the recent technologies introduced is fitting damping devices into structural members prone to seismic activities. There are different types of damping devices with different characteristics and functionality including (1) friction dampers (FDs), tuned mass dampers (TMDs), viscous dampers (VDs), and Magneto-rheological dampers (MRs). The afore-mentioned types of dampers increase the safety of buildings by dissipating the energy of seismic excitation. Thus, minimize the seismic induced stresses in any building. The functionality of these dampers is explained as follows:

Friction dampers (FDs): are designed to slip before the building structural integrity is affected. Seismic energy build up is generated within friction dampers until it overcomes the damper frictional resistance. Hence, damper surfaces slide against each other releasing heat to dissipate the energy. Friction dampers do not require replacement post any seismic activity [6-9].

Tuned mass dampers (TMD): also known as harmonic absorbers, are devices mounted in structures to reduce lateral vibrations due to seismic activities. The TMD consists of a mass mounted on one or more damped springs. The oscillation frequency of

Preprints (www.preprints.org) | NOT PEER-REVIEWED | Posted: 28 February 2023 doi:10.20944/preprints202302.0518.v1

TMD is similar to the resonant frequency of the structure it is mounted to, and reduces the structures maximum vibration under earthquake activities [10, 12].

Viscous dampers (VDs): also known as seismic dampers, are hydraulic devices used to dissipate the kinetic energy induced by earthquakes. VDs allow free and controlled damping for structures. VDs are designed and installed such that their behavior in damping vibrations depends on the excitation of the structure. Thus, VDs behavior varies when damping earthquakes or wind loading [13-16].

Magneto-rheological dampers (MR): Magneto-rheological dampers (MR-dampers) are increasingly used in construction applications to reduce the dynamic response of structures to seismic activities or severe wind loading. Sensors attached to the structure will signal the computer to supply the dampers with electric charge that transfers the MR fluid to a near-solid material with different physical and mechanical properties (viscoelastic behavior) [17-21].

The main objective of this research is to control the response behavior of specific floor(s) in a building to meet specific performance criteria under earthquake excitation using MR-dampers. The research objective is attained by optimizing the MR-dampers control parameters to attain the required response behavior. The adjustment of control parameters to attain this objective is validated in multiple case studies throughout this research. The adjustment of MR-dampers control parameters to target a given performance of specific floors resulted in optimized design of MR-dampers-installed building structures.

2. Literature Review

MR-dampers are increasingly used in seismic design of building structures, civil infrastructure [22,23], semi-active vibration isolation systems [24-26], and military vehicles [27]. MR dampers are characterized by low energy consumption for high damping forces and fast response. MR dampers depend mainly on MR fluids which is considered intelligent fluids due to their ability to change their properties when exposed to magnetic field. MR fluids main constituent includes the carrier fluid, magnetic particles, and additives. Carbonyl iron, with 99% purity, is often used as magnetic particles due to its high magnetic permeability [28]. In some MR-dampers, carbonyl iron particle size range between 3 to 5 microns and a concentration ranging from 20% to 40%. Thus, the likelihood of corrosion of the MR-damper outer surface is minimal [29]. When a magnetic field is applied on the MR-fluid, the fluid rheological properties changes, and the shear capacity of the fluid increase. The magnetic field is applied by a wire coil embedded within the damper [30]. A detailed diagram of MR-damper function is shown in Figure 1, and MR-damper structure is shown in Figure 2.

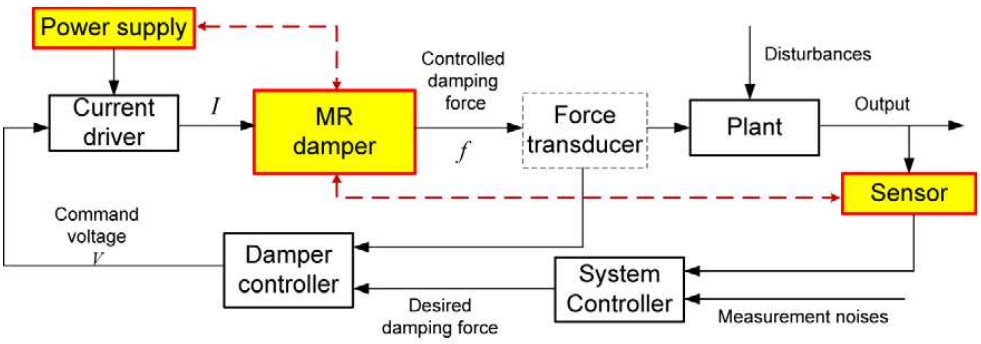

Figure 1. Schematic diagram of MR-damper semi-active control system [31]

Preprints (www.preprints.org) | NOT PEER-REVIEWED | Posted: 28 February 2023 doi:10.20944/preprints202302.0518.v1

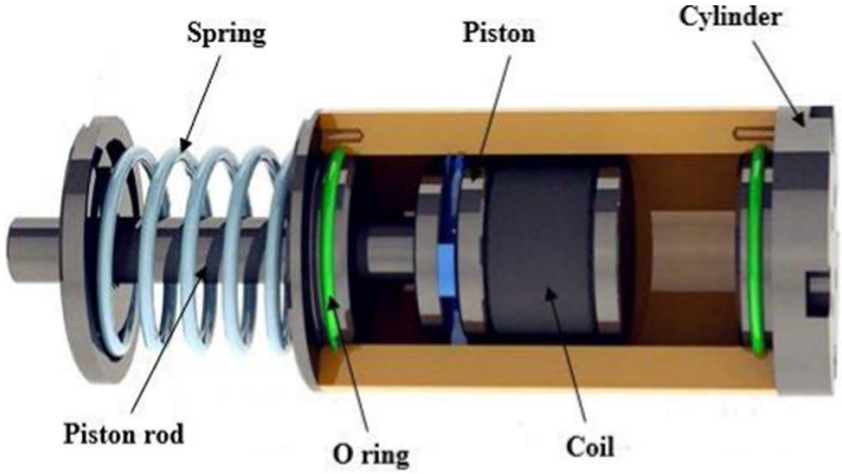

Figure 2. MR-damper structure [32]

Researchers investigated different strategies to control MR-dampers. In a relevant research study, researchers proposed using clipped-optimal (CO) controller and a Lyapunov controller control. The study investigated the behavior and response of a six-story test structure with four shear mode MR-dampers, two dampers placed between the base and the first floor, and two dampers placed between the first and the second floor. Results obtained from experimental data were comparable to an equivalent passive control system control MR-dampers to reduce structural response due to seismic loads.

In 2002 Yang et al. presented the dynamic model of the damper [33], later in 2004 they extended the dynamic model to include the phenomenological model of the damper demonstrating the MR-damper potential for practical civil engineering applications [34]. In 2003 Fujitani et al. [35] developed a 400kN bypass type damper for base isolated buildings, using a new MR fluid. Experimental testing validated the dynamic model and the capacity of the developed damper. Later in 2013 MR-damper design with numerical example for shear-valve mode was carried out by Xu, et al. [36] where they designed and tested a 200kN damper. Onoda and Oh et al. [12, 13] demonstrated the superiority of MR-dampers (flow bypass type) over ER dampers at suppressing the vibration of a 10-bay truss system.

Control algorithms play a key role for the structurally controlled buildings. in a comparative study conducted in 2000. Jansen and Dyke [37] presented the results of a series of control algorithms applied to MR-dampers for a six-story numerical model. Later more advanced control algorithms based on fuzzy controllers emerged. These algorisms can produce optimized performance such as the ones presented by Choi, et al. [15] in 2004. And by Bhardwaj and Datta [38] in 2006. by 2010 direct adaptive controller was presented by Bitaraf, et al [39]. In 2011 genetic based fuzzy controller was presented by Cetin et al. [18]. In 2013 Ali [40] presented Quasi-Bang-Bang controller with fuzzy logic-based input for the driver voltage and in 2019 Bozorgvar and Zahrai [41] presented adaptive neural-fuzzy intelligent controller optimized using genetic algorithm.

In 2018, Bathaei et al. [42] presented an 11-DOF building with toned mass damper and two MR-dampers and fuzzy control algorithm to evaluate their capacity in seismic mitigation compared to the uncontrolled building. Later in 2021 Bagherkhani and Baghlani [43] presented a reliability assessment of MR-dampers for two cases: structural safety, and human comfort when used in the semi active and passive modes. Also, Fakhry et al. [44] presented an optimized response for a practical high-rise structure modeled using mixed finite element method and boundary element method (BEM) for 9 and practical building 20 floors. The authors in [44] used a control algorithm based on the clip optimal approach and variable voltage for the current driver approach.

Preprints (www.preprints.org) | NOT PEER-REVIEWED | Posted: 28 February 2023 doi:10.20944/preprints202302.0518.v1

In this research, the previous methodology developed by Fakhry et al. [44] is implemented using a graphic user interface (GUI). The GUI exploits the full potential to guide the control parameters for an optimized response. This guidance is performed to satisfy a specific floor or set of floors design criteria. The new setup is evaluated for potential favorable control output using practical buildings and earthquakes both synthetic and historical.

In order to facilitate current testing and future utilization, the GUI was also split into three modes, as follows:

Design mode: using one earthquake to generate control parameters
Simulation mode: to produce controlled response for new earthquakes
Acting mode: which is a code generated to be installed on a special purpose computer or a micro controller to apply voltage to MR-Dampers in situ.

3. Graphical User Interface (GUI) Smart Control

To facilitate the validation of the proposed scheme, several steps were defined. First, an interface for the smart controller is developed. The interface is split into two tabs:

First tab (Design Mode) contains all required data input parameters for the design of MR-damper placement as presented in Figure 3. After the building properties directory is selected and all required structural data is loaded in GUI first container (1. Building Properties Directory), earthquake for design mode is either selected from earthquakes used in previous dynamic analysis of building or the user can select a new design earthquake in GUI second container (2. Loading Design EQ).

In the third container of the GUI (3. Floors and Damper Factors R-Q): the user defines the floors with potential damper placement and defines the upper and lower bounds for the R control parameter passed to the PSO according to required design criteria, also, the upper and lower bounds for the Q control parameter to be passed to the PSO.

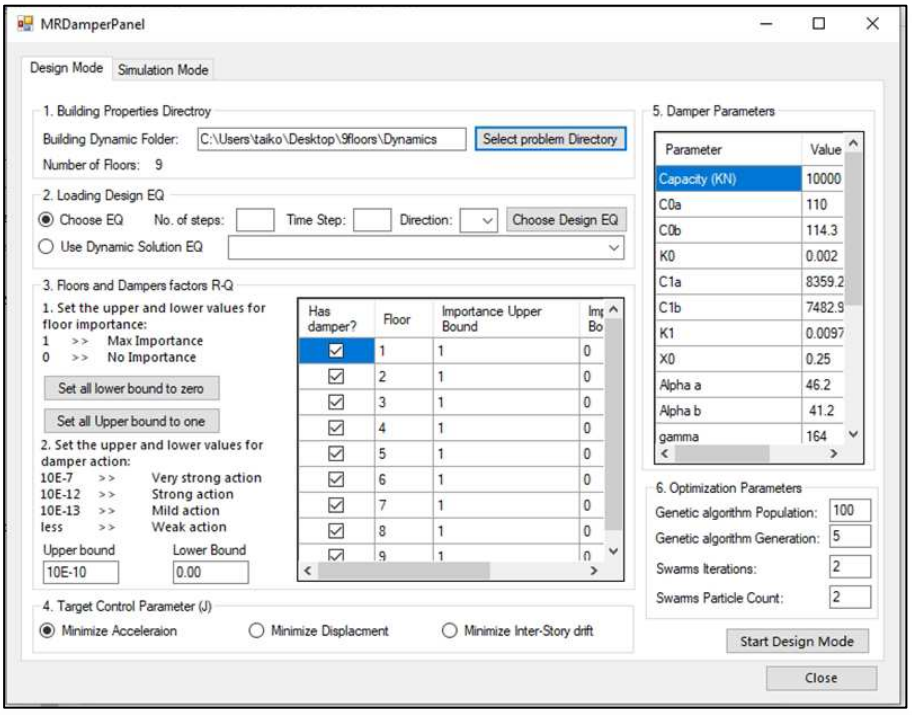

Figure 3. Design mode graphical user interface (GUI)

Preprints (www.preprints.org) | NOT PEER-REVIEWED | Posted: 28 February 2023 doi:10.20944/preprints202302.0518.v1

In the fourth container (4. Target Control Parameter J) the target response minimization type is selected from three evaluation criteria: Displacement, Acceleration, and Inter-story drift, these three options correspond to J_1, J_2, and J_3 respectively defined in previous research [45]. The GA target objective function changes according to user input. In container 5 (Damper Parameters) the user inputs the MR-damper parameters according to the modified Boch-Wen model presented in Appendix B.
The last container (5. Optimization Parameters) contains the desired GA optimization population and generations count, and the PSO number of iteration and particle count.
After filling all required data, the user starts the design mode presented in detail in section 3 (Control Scheme).

The second tab (Simulation Mode) presented in Figure 4 collects the available earthquakes from previous dynamic analysis. In addition, it allows the user to add new earthquakes for simulation. After selecting one or several Earthquake files, the controlled response of the building for the selected earthquake is generated using previously produced control gain parameters and damper location generate. The simulation mode operation is presented in the following section.

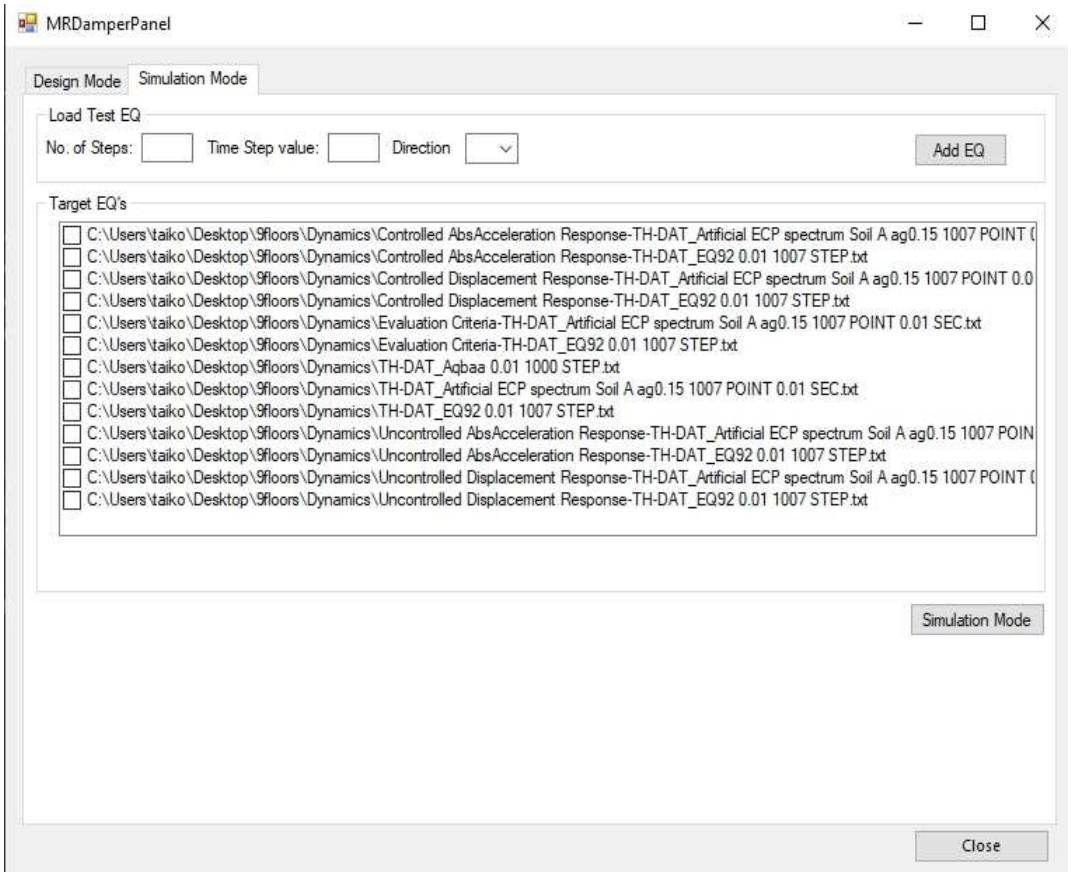

Figure 4. Simulation mode

4. The Control Scheme

Fakhry et al. [37] presented the force ratio-based voltage control scheme is implemented for this study, in this approach, the voltage for the MR force is calculated based on the ratio between the current force in damper (f) and the desired control force (f_c) as presented in Eqn. 5, the graduation of voltage change proved a more efficient compared to the CO approach.

Preprints (www.preprints.org) | NOT PEER-REVIEWED | Posted: 28 February 2023 doi:10.20944/preprints202302.0518.v1

$$V = \begin{cases} \left(1 - \frac{f}{f_c}\right) V_{max} & f < f_c \\ 0, & f > f_c \end{cases} \quad (1)$$

The operation scheme is split into three modes of operation the first mode is as described in the previous section, where the software controls the response of a building for a given earthquake, the output of this mode is a controlled building response, dampers locations, and control gain weighting matrices (R and Q) (see Appendix A).

The second mode is simulation mode, a new Earthquake along with previously generated damper locations and control gain weighting matrices (R and Q), using previously generated building data, controlled response is generated for the new Earthquake.

The third mode is an embedded system operation, this mode is like the simulation mode, but all variables for the software (i.e., building stiffness matrix, mass matrix, damping matrix, control gain parameters, damper locations, and electric current ports) are static and imbedded in the system except for sensor data which is obtained directly from accelerometer sensors located at each floor. Earthquake record is obtained from the national seismic network or directly from nearby seismological recoding station.

4.1. Design mode

Figure 5 presents the overall control flow of the software implemented, the software begins by obtaining building data resulted from the Boundary element method and Finite element method (BEM/FEM) analysis performed in BIM environment [46], Earthquake data is also loaded into the same environment.

State-Space representation of the building is generated without control forces. The next step for the software is to obtain the values for the parameters of the MR-Damper, the parameter for the genetic algorithm, and the parameters for the particle swarm algorithm (PSO) [47].

The main program loop is the genetic algorithm, the genetic algorithm generates an individual, this individual element is a set of trial locations for the MR-Damper and feeds the damper location to the second loop of the software the PSO, the PSO optimizes the control algorithm Linear Quadratic Gaussian (LQG) by changing the weighting matrices Q and R, the PSO runs the control algorithm and estimates control gain parameters Q and R in the process to minimize a fitness function J. (See Appendix A). These control parameters are stored for each iteration of the PSO. Finally, after finding the best operation control gain and best damper locations, the best damper locations are stored, and the controlled response of the building is generated and stored.

4.2. Simulation mode

The simulation mode is presented in figure 6, the resulted control gain, damper location, and building parameters, are combined with a new earthquake and produce the corresponding controlled response.

4.3. Acting mode

The acting mode presented in figure 7 is a fixed code to be installed on a Special Purpose Computer (SPC) or a digital controller, building properties including Stiffness matrix, Mass matrix, and damping matrix are stored in fixed format in the SPC, also the weighting matrices R and Q generated from the design mode, after sufficient iteration for the double optimization scheme. Sensors to be installed for the building, the number of sensors is obtained from the GA best individual. When the structure is excited from an earthquake, the current driver provides voltage to MR-dampers matching the resulted voltage required to mitigate building response according to the building response type, which is also stored on the SPC.

Preprints (www.preprints.org) | NOT PEER-REVIEWED | Posted: 28 February 2023 doi:10.20944/preprints202302.0518.v1

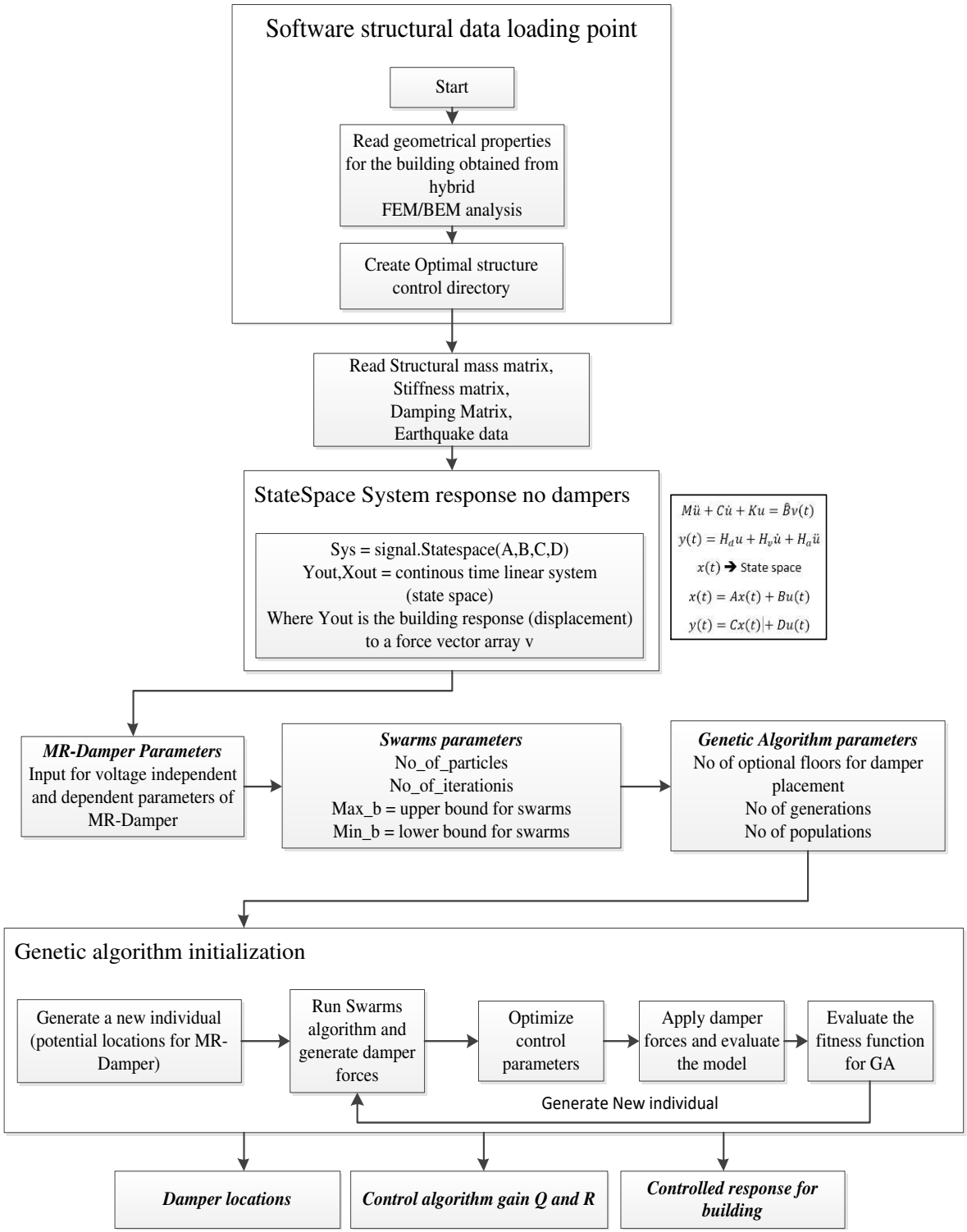

Figure 5. Flow chart for the control scheme (design mode)

Preprints (www.preprints.org) | NOT PEER-REVIEWED | Posted: 28 February 2023 doi:10.20944/preprints202302.0518.v1

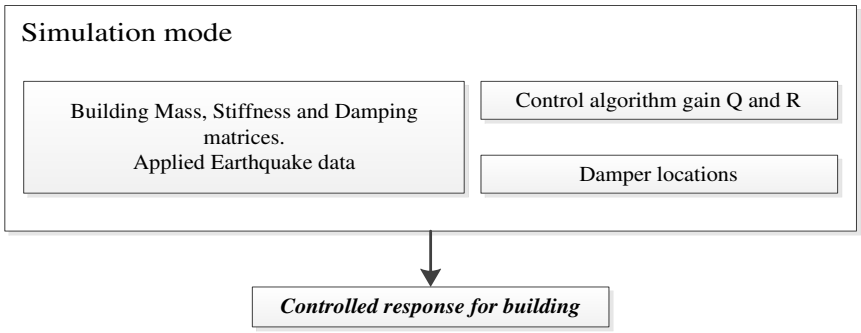

Figure 6: Simulation mode

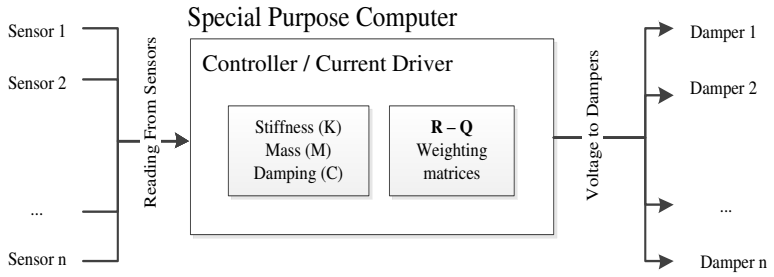

Figure 7. The schematic for the operation of the acting mode.

5. Case Study

For the study of changing the control gain parameters and changing the target response type for minimizing, two buildings were selected figure 8 presents the typical plan of the buildings, the building is 40 times 32 meters with 49 columns, 2 three-sided cores, and three openings.

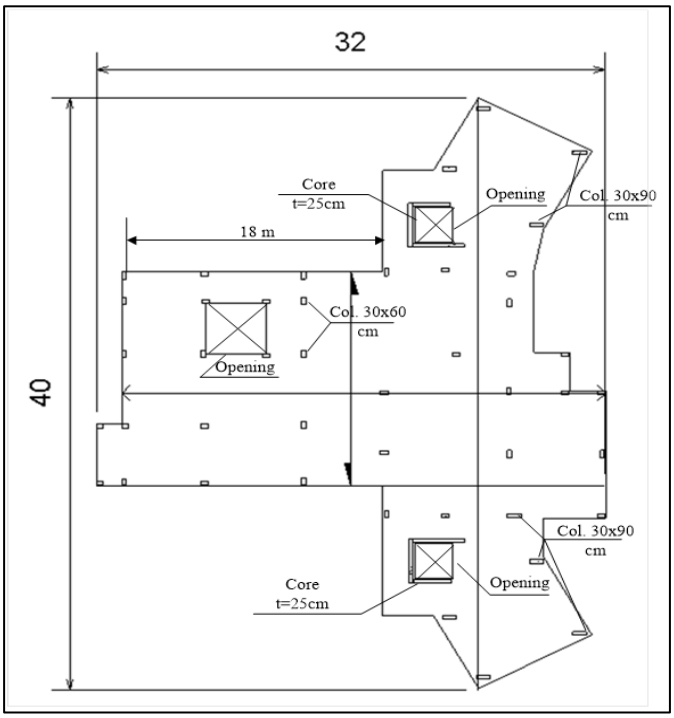

Figure 8. Typical floor plan for the study buildings.

Preprints (www.preprints.org) | NOT PEER-REVIEWED | Posted: 28 February 2023 doi:10.20944/preprints202302.0518.v1

Figures 9 present the 3D view of the buildings (18 floors and 9 floors) with typical floor height 3 meter.

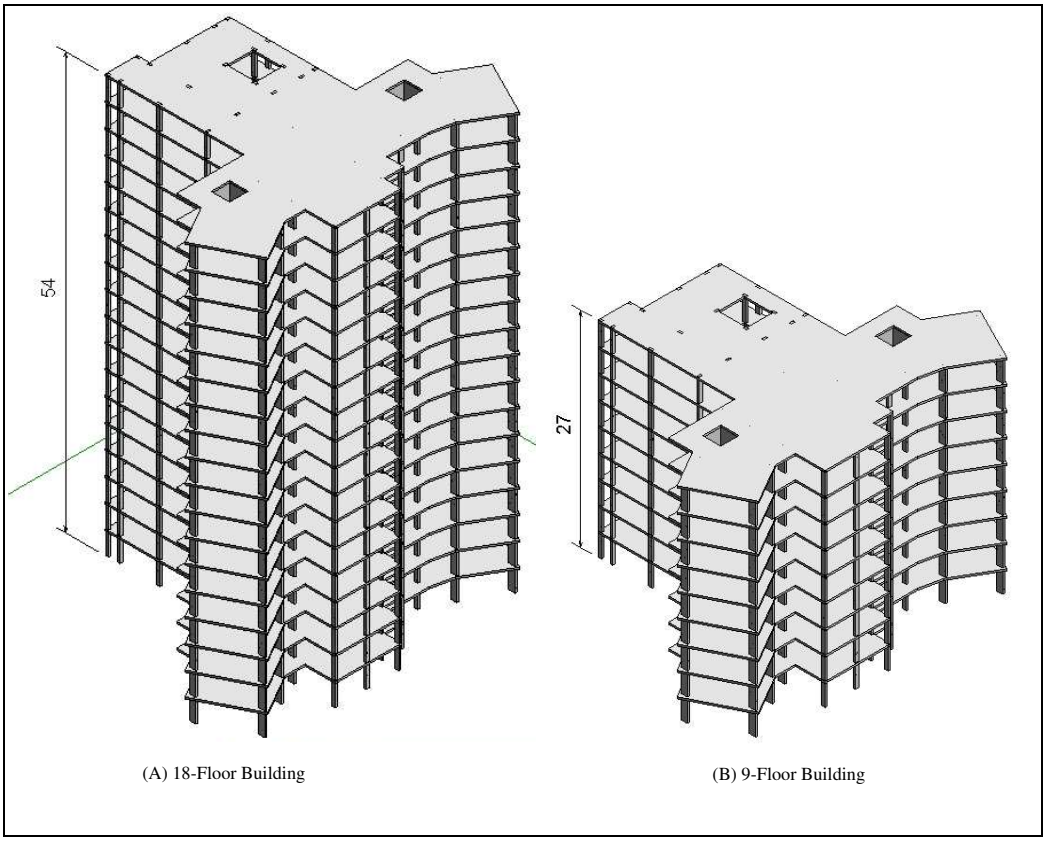

Figure 9. 18-floor building and 9-floor building.

Earthquakes are selected in two different locations for the investigation: Egypt and USA, the design response spectrums for both locations are used to generate synthetic earthquakes. All acceleration values are expressed in meter/sec^2 on the Y axis and seconds in X axis. The Egyptian Earthquake generated with a_g=0.15g (base ground acceleration) and Soil Type A. This Earthquake is plotted in figure 10. And ASCE Earthquake generated for Soil Type C and S_s=0.6 and S_1= 0.32 and plotted in figure 11. Historical Earthquakes El Centro 1940, Northridge 1994, Egypt 1992 and Aqaba 1995 are presented in figures 12,13,14 and 15 in terms of acceleration in m/sec^2

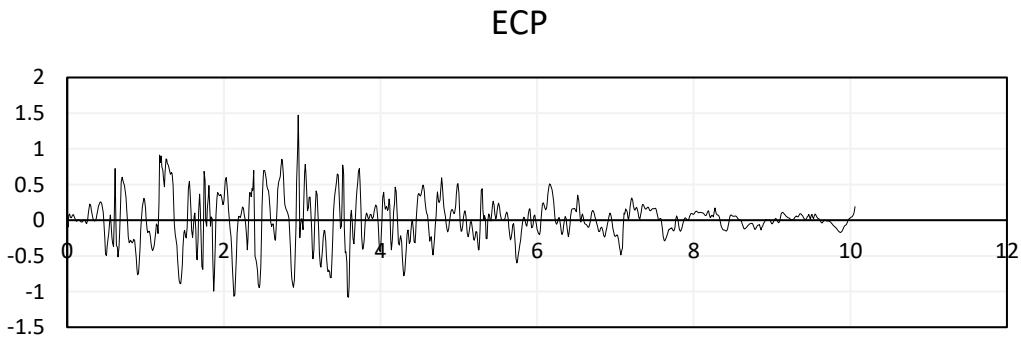

Figure 10. Synthetic earthquake generated from ECP

Preprints (www.preprints.org) | NOT PEER-REVIEWED | Posted: 28 February 2023 doi:10.20944/preprints202302.0518.v1

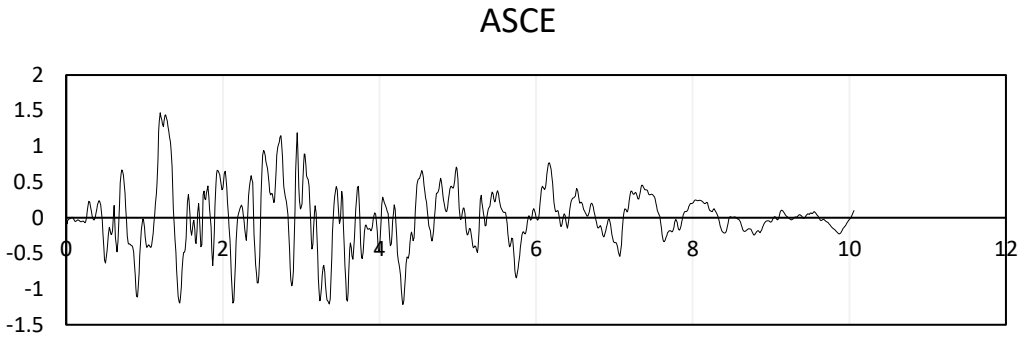

Figure 11. Synthetic earthquake generated from ASCE

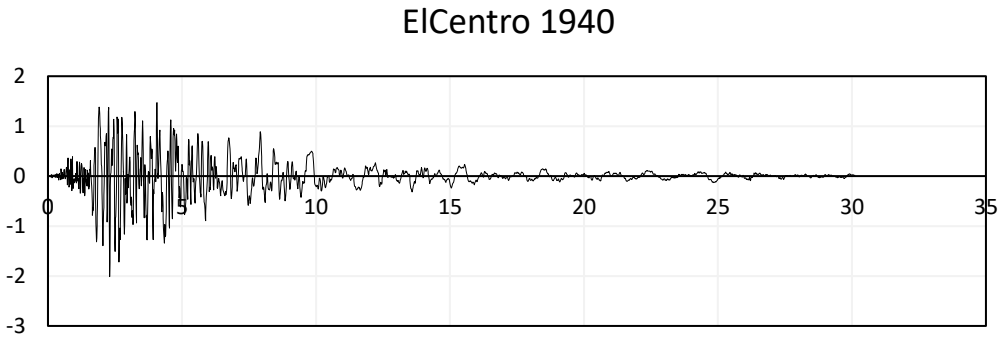

Figure 12. El Centro 1940 earthquake

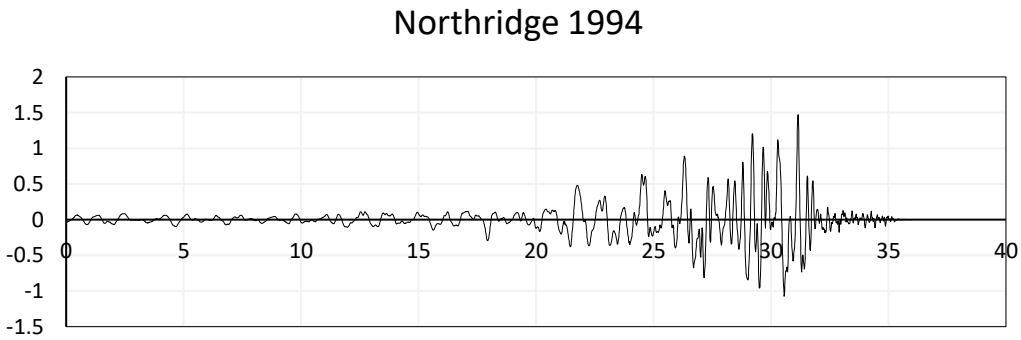

Figure 13. Northridge 1994 earthquake

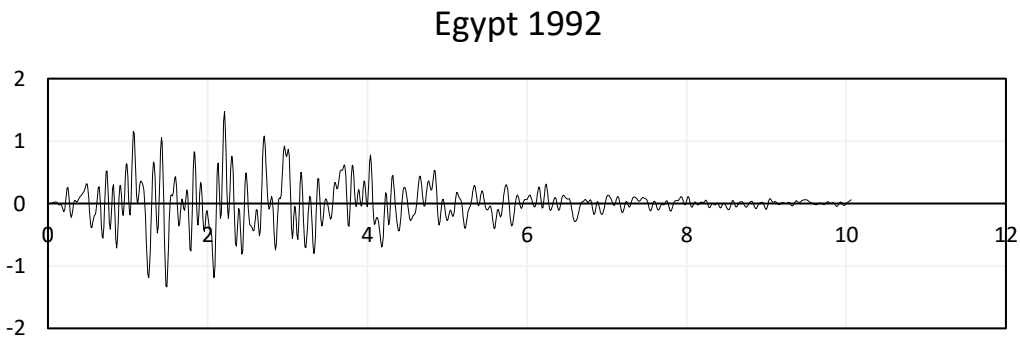

Figure 14. Egypt 1992 earthquake

Preprints (www.preprints.org) | NOT PEER-REVIEWED | Posted: 28 February 2023 doi:10.20944/preprints202302.0518.v1

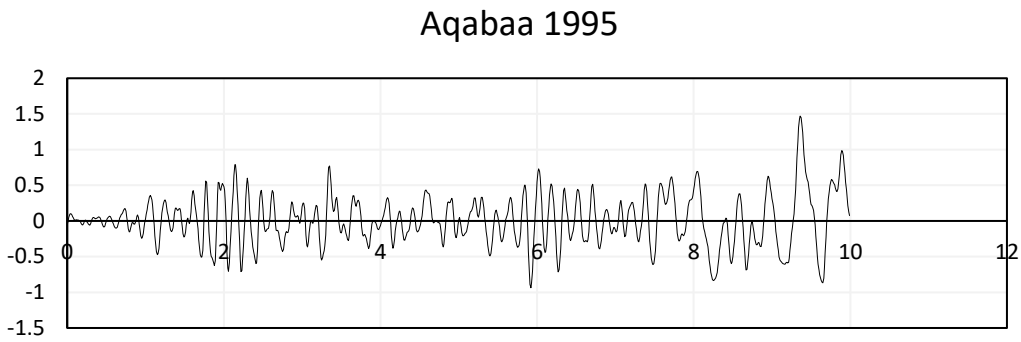

Figure 15. Aqaba 1995 earthquake

The GUI allows for three types of target response optimization: J_1, J_2, and J_3. Switching between the three values changes the target optimization function for the GA. Twelve tests were carried out for the two buildings, 12 design runs are preformed using the artificial response spectrum generated earthquakes. For reach building, once using the ECP earthquake and once using ASCE earthquake where the target response optimization is set to each of the three target responses. 24 simulation mode models were carried, for each building in each of the two location, two local earthquakes are simulated for each of the three responses. Table 1 presents a summary of the analysis for the GA approach, where the letter D donates design mode, and the letter S donates simulation mode.

Table 1: GA target Response optimization change scheme

	Building 1 (9 floors)			Building 2 (18 floors)		
Target Response	Acc.	Disp.	Inter-story Drift	Acc	Disp.	Inter-story Drift
ECP	D	D	D	D	D	D
ASCE	D	D	D	D	D	D
Egypt 92	S	S	S	S	S	S
Aqabaa	S	S	S	S	S	S
Northridge	S	S	S	S	S	S
El Centro	S	S	S	S	S	S

5.1. PSO floor-specific control weighting parameters change

The GUI allows for the change of POS ranges regarding the R and Q weighting matrices, the R weighting matrix is directly linked to the controlling force i.e., MR-damper action force, the PSO algorithm is allowed to change the R value freely. Meaning that there are no constraints applied to the damper force, since the maximum force in damper is already limited to the damper model (Presented in appendix B).

For the Q weighting matrix, the PSO input range for each floor of the building is set to the range (0, 1) by default. The PSO range is changed to (0.9, 1) when the significance of a specific floor of the building needs to be increased, to the overall structural behavior in terms of displacement, this practice is carried out for an array of possible scenarios. This scheme is performed 4 times, once for each of the two buildings and once in for each of the artificial earthquakes.

Each case has one design mode using the artificial earthquake and two simulation modes using the provided earthquakes for each design code of practice region.

Preprints (www.preprints.org) | NOT PEER-REVIEWED | Posted: 28 February 2023 doi:10.20944/preprints202302.0518.v1

Table 2: The selected floors for the Q modification scenarios

	Building 1 (9 floors)	Building 2 (18 floors)
Case	Target floors	Target floors
1	3	6
2	6	12
3	9	18
4	3, 6	6, 12
5	3, 6, 9	12, 18
6	6, 9	6, 12, 18
7	3, 4	6, 7
8	3, 4, 5	6, 7, 8
9	6, 7	12, 13
10	6, 7, 8	12, 13, 14
11	2, 3, 4, 5	4, 5, 6, 7
12	6, 7, 8, 9	12, 13, 14, 15

6. Selected Results and Discussions

Figures 16 and 17 present the base case for forces in damper when the 9-story building is subjected to the ECP EQ and ASCE EQ respectively, reduction in displacement response is at 52% for the ECP EQ and 50% for ASCE EQ. The second case had more maximum displacement and consequently more damping force.

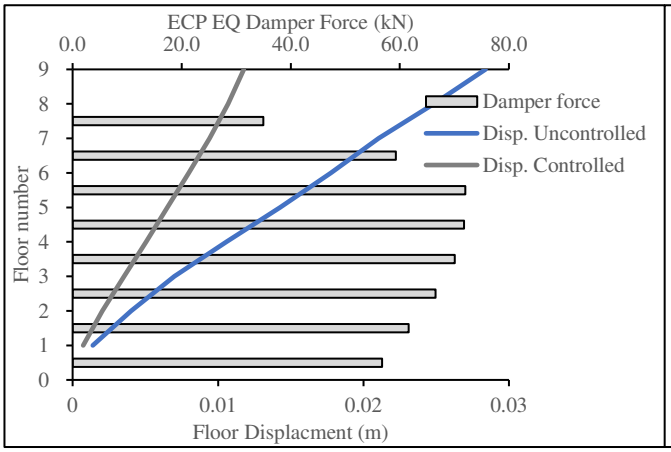

Figure 16. Displacement reduction for ECP EQ

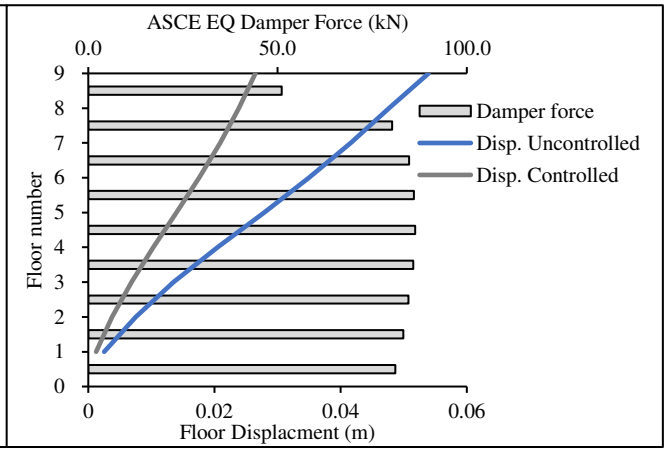

Figure 17. Displacement reduction for ASCE EQ

For Figures 18 and 19 the target response type is changed to acceleration and compared to the acceleration resulted form the base case (displacment case). The results showcase the success in producing lower acceleration response, achieving the targeted results.

Preprints (www.preprints.org) | NOT PEER-REVIEWED | Posted: 28 February 2023 doi:10.20944/preprints202302.0518.v1

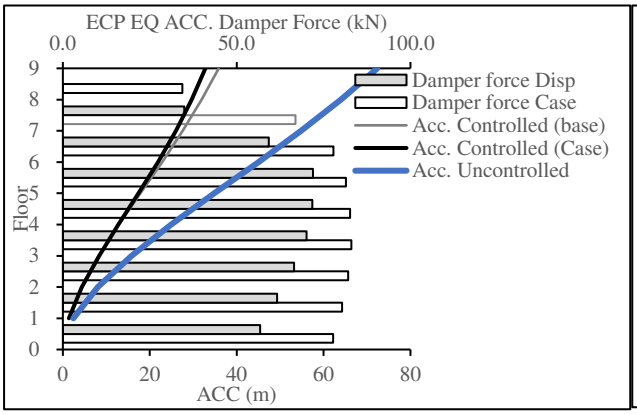

Figure 18. Acceleration reduction for ECP EQ

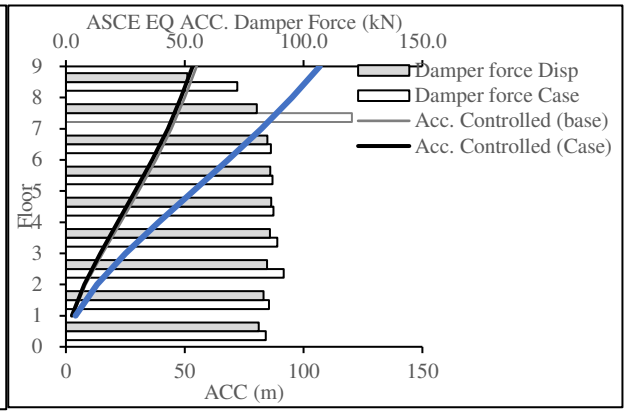

Figure 19. Acceleration reduction for ASCE EQ

For Figure 20 and 21 the target response type is changed to inter-story drift and compared to the inter-story drift resulted from the base case (displacement case). The results showcase the success in producing lower inter-story drift response, achieving the targeted results.

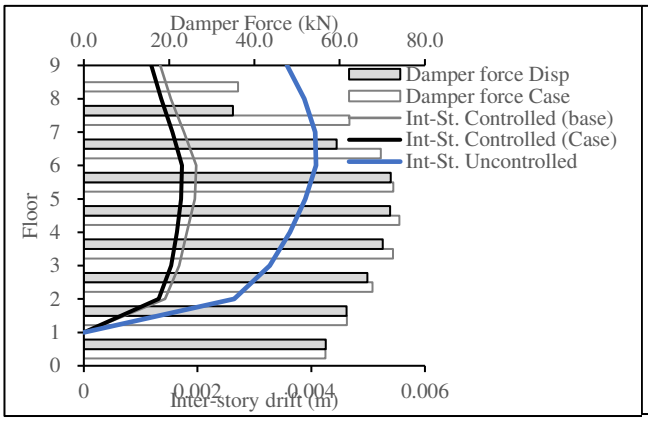

Figure 20. Inter-story reduction for ECP EQ

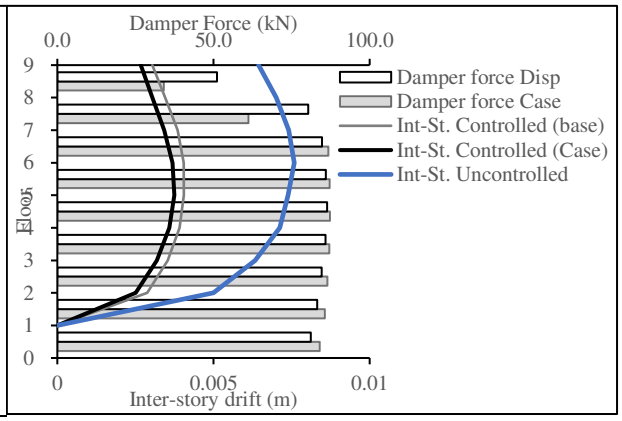

Figure 21. Inter-story reduction for ASCE EQ

Figures 22 and 23 present the base case for forces in damper when the 9-story building is subjected to the ECP EQ and ASCE EQ respectively, reduction in displacement response is at 54% for the ECP EQ and 42% for ASCE EQ. The second case had higher maximum displacement and consequently more damping force.

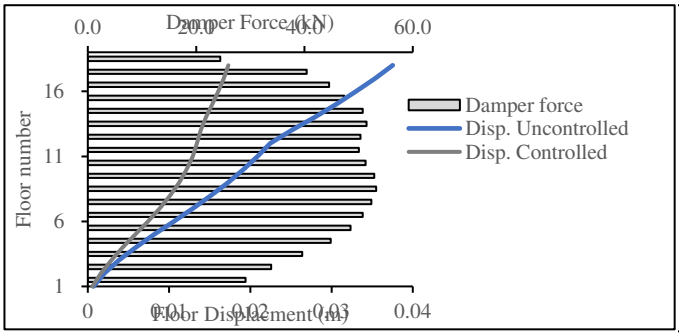

Figure 22. Displacement reduction fro ECP EQ

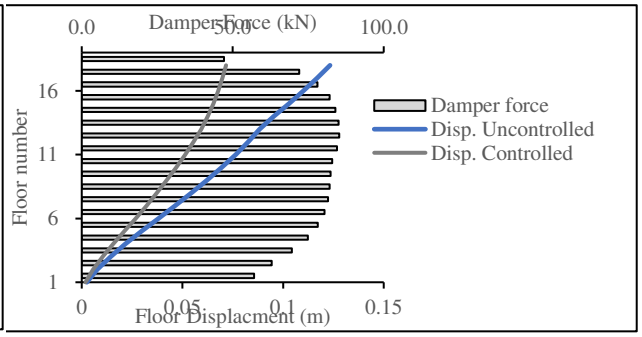

Figure 23. Displacement reduction for ASCE EQ

Preprints (www.preprints.org) | NOT PEER-REVIEWED | Posted: 28 February 2023 doi:10.20944/preprints202302.0518.v1

For Figures 24 and 25 the target response type is changed to acceleration and compared to the acceleration resulted from the base (displacement case). The results showcase the success in producing lower acceleration response, achieving the targeted results.

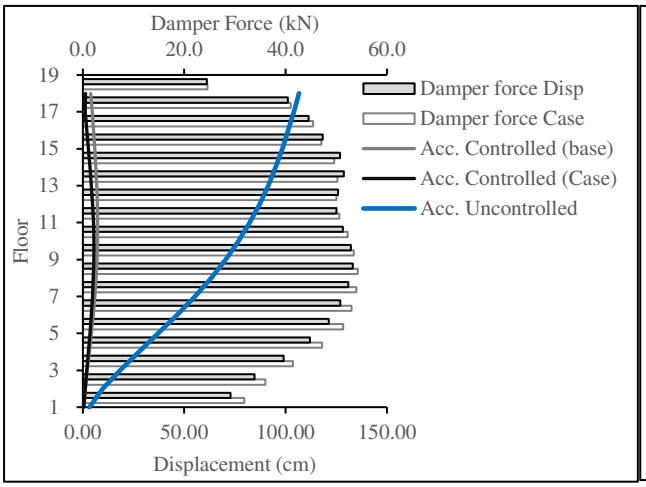

Figure 24. Acceleration reduction for ECP EQ

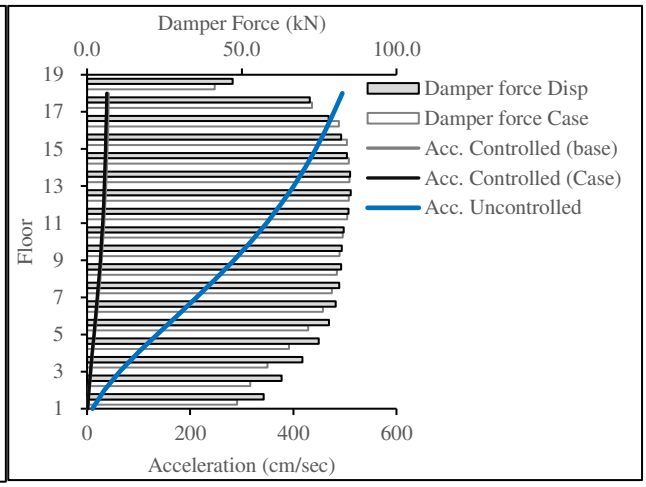

Figure 25. Acceleration reduction for ASCE EQ

For Figures 26 and 27 the target response type is changed to inter-story drift and compared to the inter-story drift resulted from the base case (displacement case). The results showcase the success in producing lower inter-story drift response, achieving the targeted results.

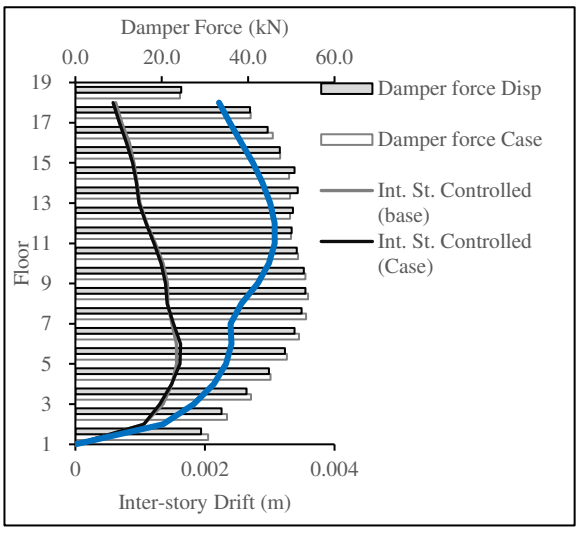

Figure 26. Displacement reduction for ECP EQ

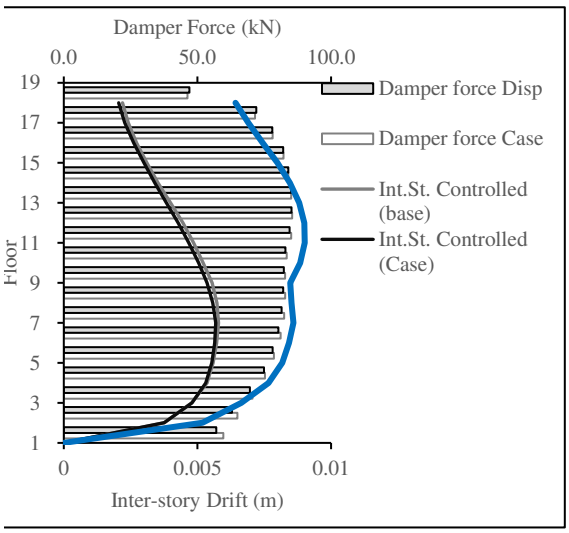

Figure 27. Inter-story drift reduction for ECP EQ

The rest of the figures present a selected collection of cases of choosing a single or multiple floors to guide the optimization algorithm towards reducing the displacement response for the chosen floor(s). From the presented results, it can be observed that clustering the target reduction for several consecutive floors presented more favorable results than scattering the selection or selecting a single floor for response reduction.

Preprints (www.preprints.org) | NOT PEER-REVIEWED | Posted: 28 February 2023 doi:10.20944/preprints202302.0518.v1

9 floors

CASE 1

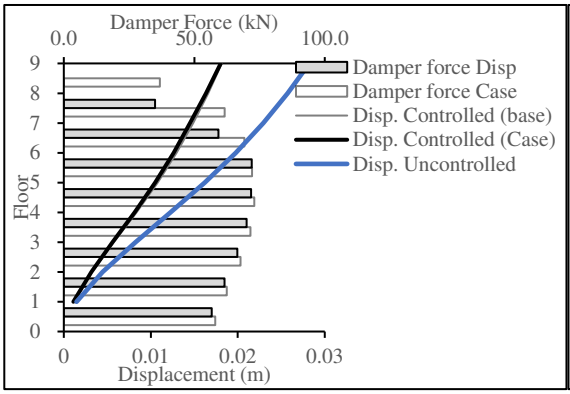

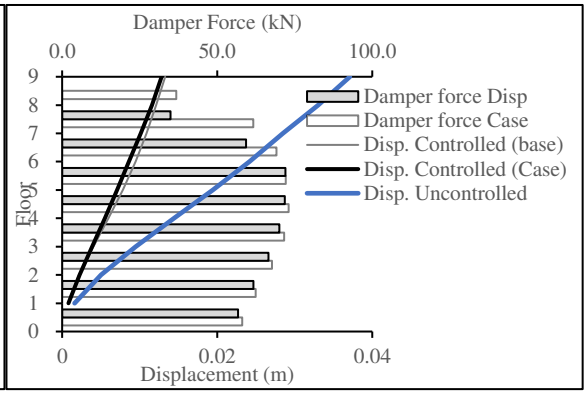

CASE 1

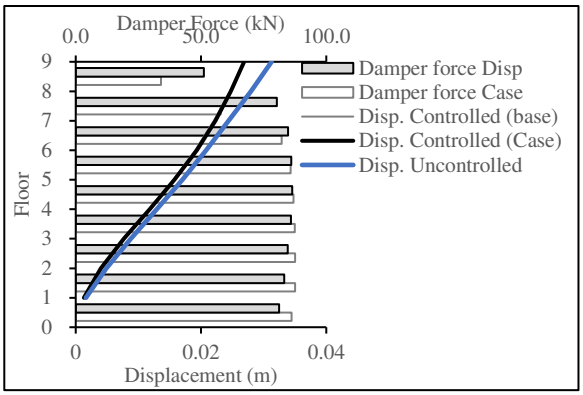

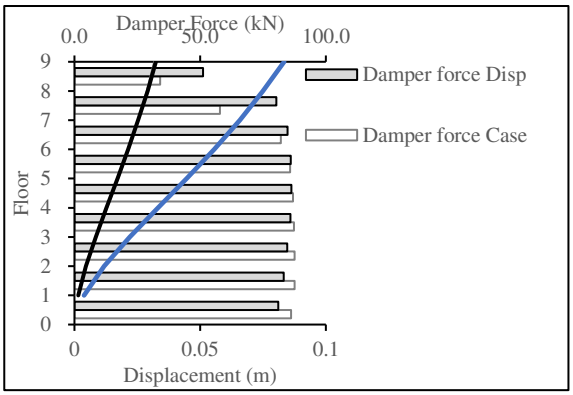

CASE 8

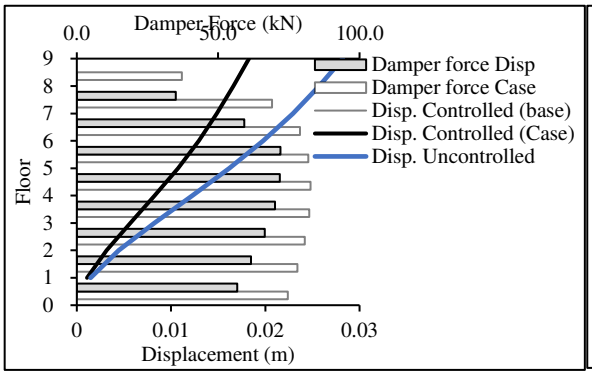

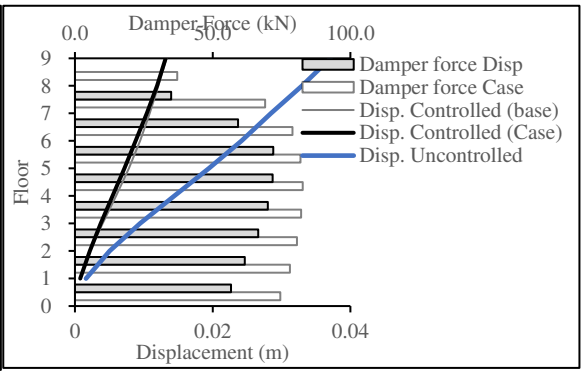

CASE 8

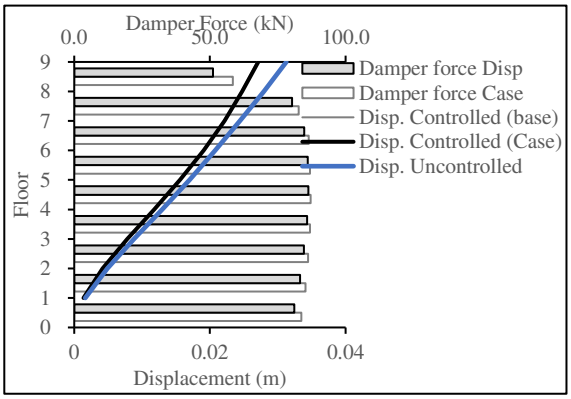

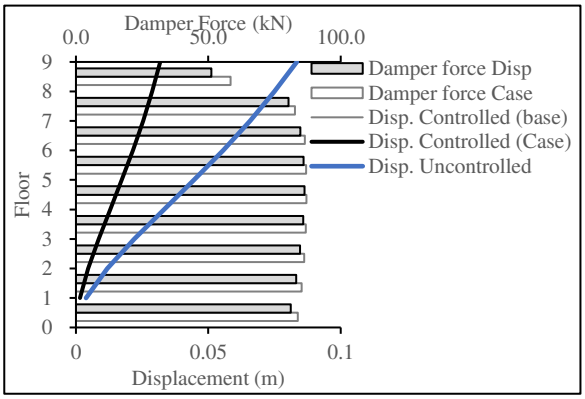

Preprints (www.preprints.org) | NOT PEER-REVIEWED | Posted: 28 February 2023 doi:10.20944/preprints202302.0518.v1

CASE 5

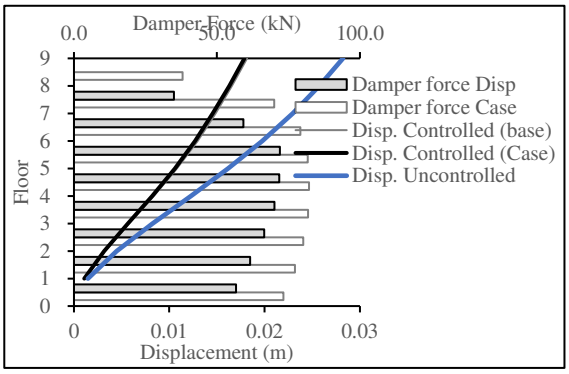

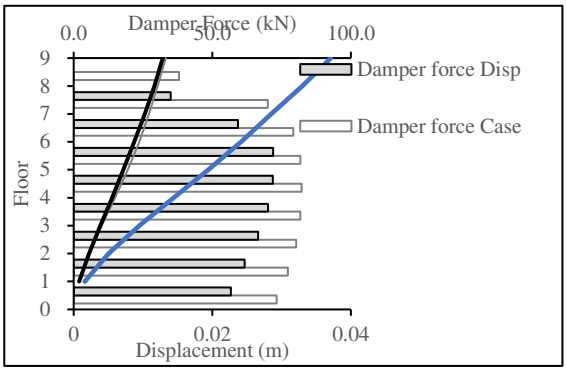

CASE 5

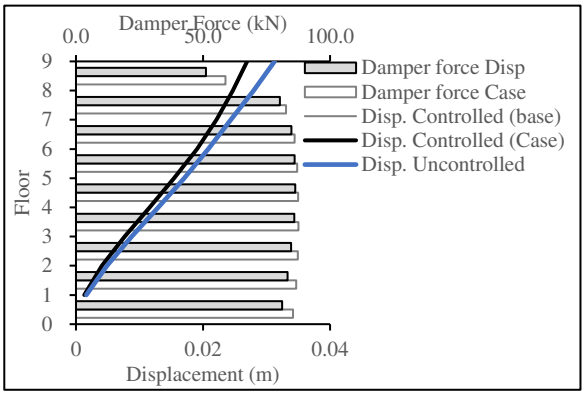

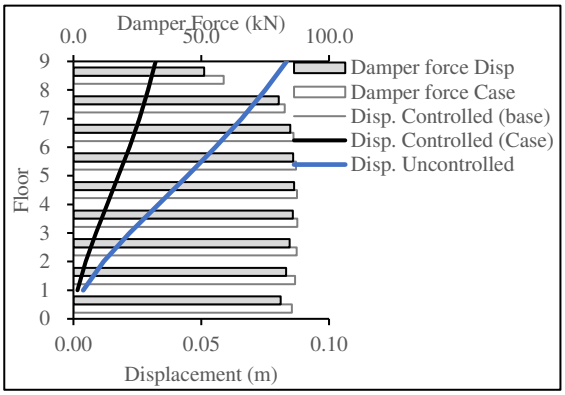

CASE 11

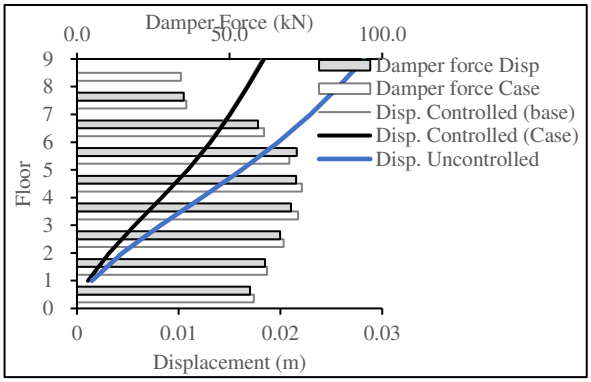

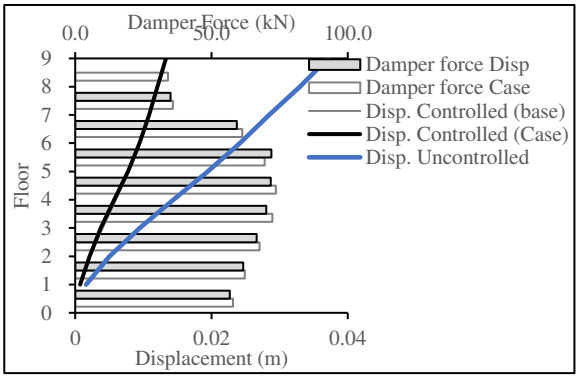

CASE 11

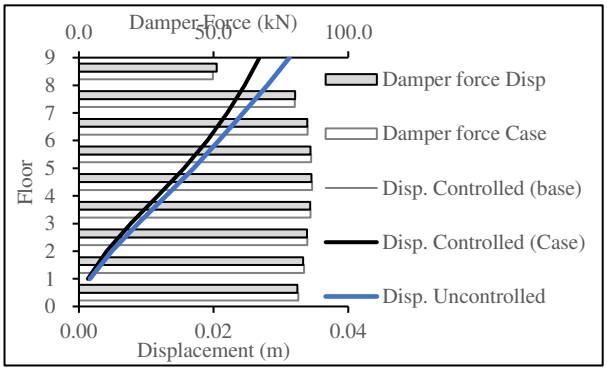

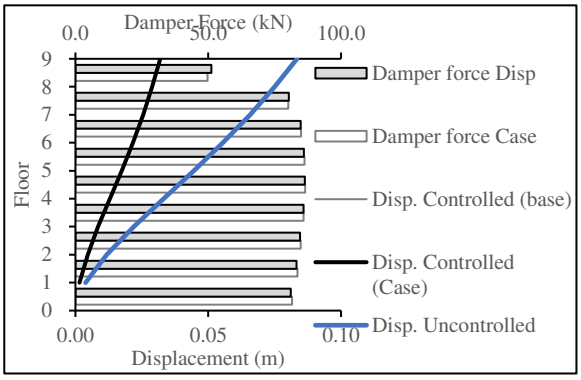

Preprints (www.preprints.org) | NOT PEER-REVIEWED | Posted: 28 February 2023 doi:10.20944/preprints202302.0518.v1

18 floors

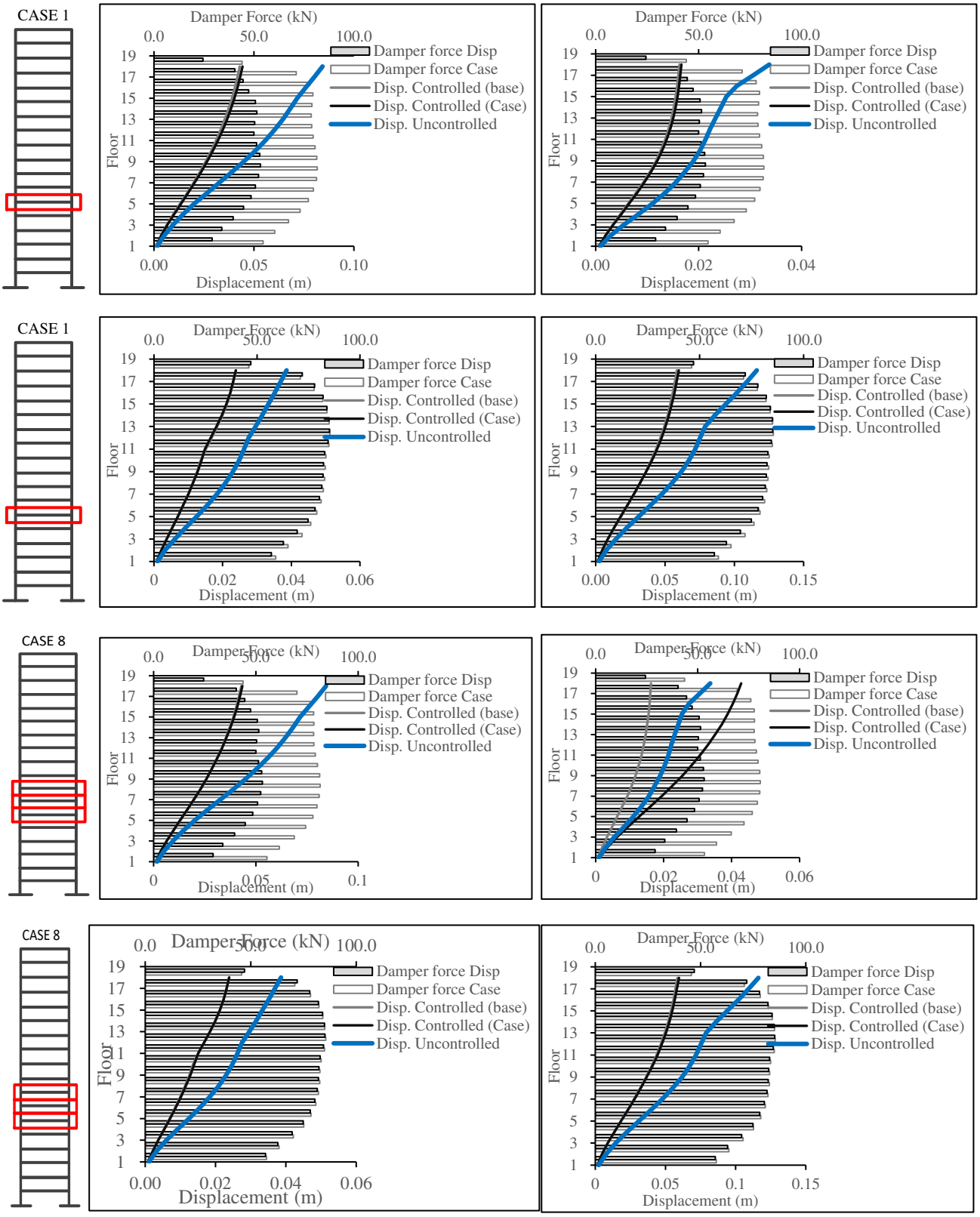

Preprints (www.preprints.org) | NOT PEER-REVIEWED | Posted: 28 February 2023 doi:10.20944/preprints202302.0518.v1

CASE 5

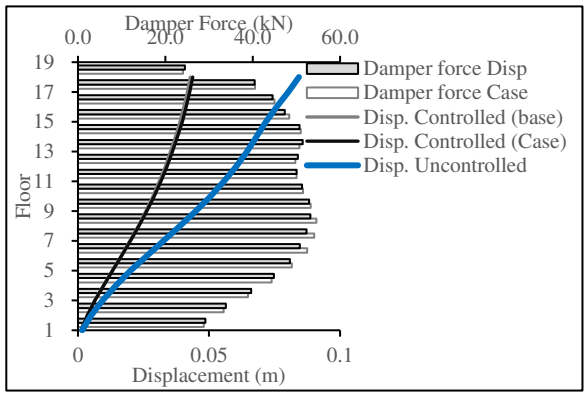

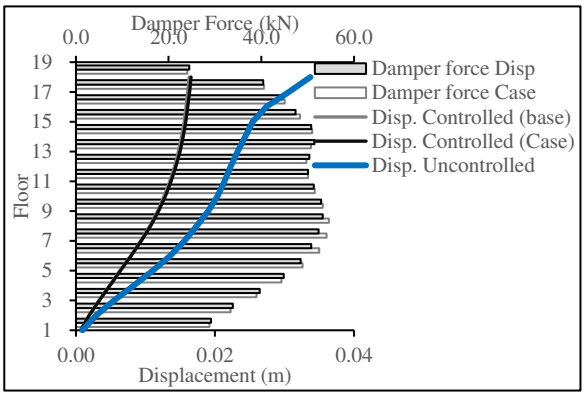

CASE 5

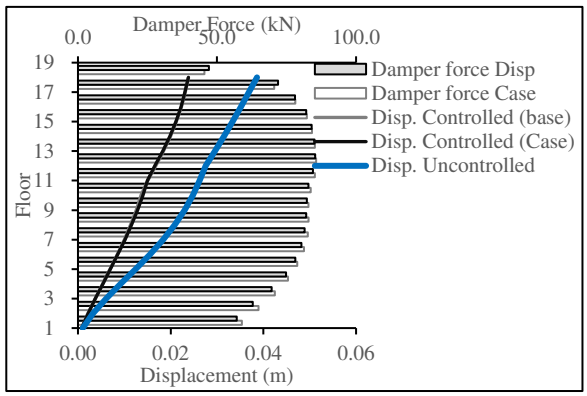

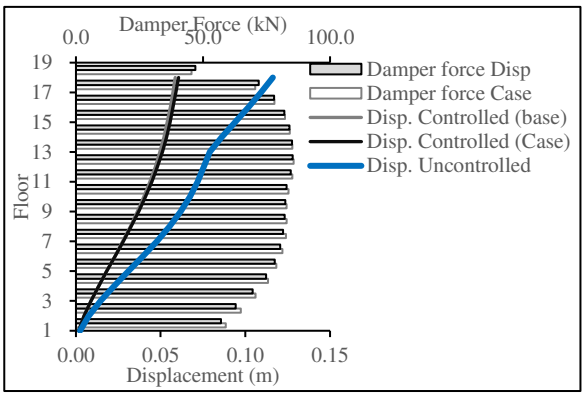

CASE 11

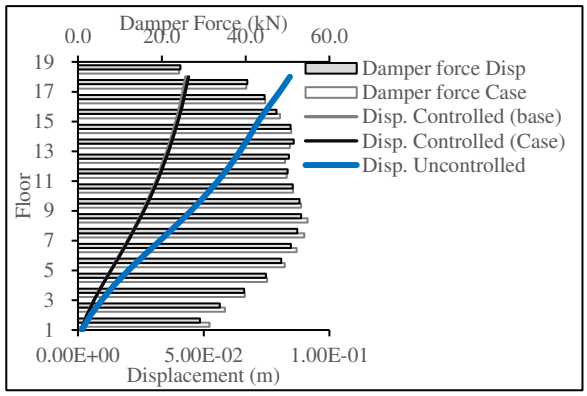

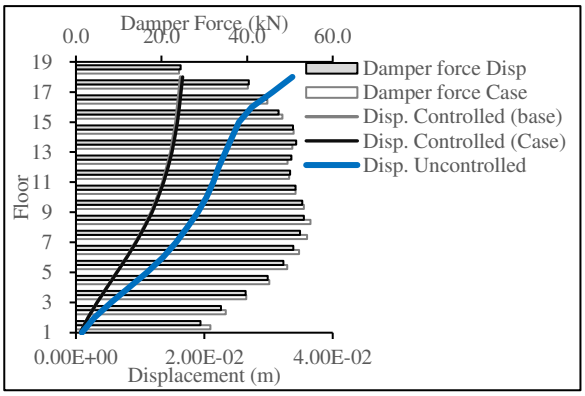

CASE 11

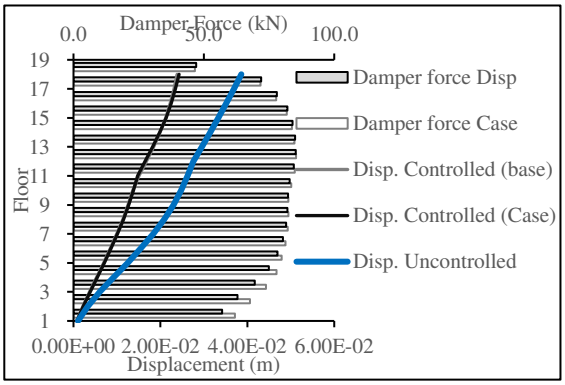

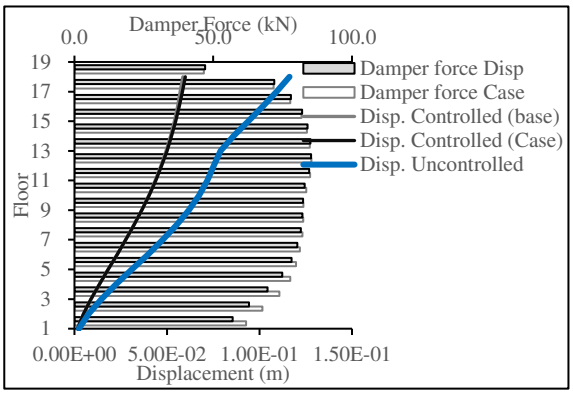

7. Conclusions

The development of the GUI streamlined the design objectives guiding of the process for MR-dampers placement in tall buildings, LQG algorithm weighting matrices R and Q are constrained using a simplified interface that guides the PSO to produce favorable outcomes for specific floors in the structure. From the presented results it can be concluded that the best practice for a Target behavior for a specific floor or set of floors is to cluster the Q bounding values in the GUI, this usually increases the forces in MR-Dampers at the specific floor or set of floors and below. Target optimization J is adjusted to present three types of seismic response outcome: acceleration, displacement, and inter-story drift with success.

Funding

This project was supported financially by the Science and Technology & Innovation Funding Authority (STIFA), Egypt, Grant No. 37145

References

1. El-Helou, R., and Graybeal, B.A. Flexural behavior and design of ultra-high-performance concrete beams. ASCE Journal of Structural Engineering, 2022, Vol. 148, No. 4 DOI: 10.1061/(ASCE)ST.1943-541X.0003246
2. Akhnoukh, A.K., and Buckhalter, C. Ultra-high-performance concrete: constituents, mechanical properties, applications, and current challenges. Case Studies in Construction Materials, 2021, Vol. 15 https://doi.org/10.1016/j.cscm.2021.e00559
3. Akhnoukh, A.K., and Elia, H. Developing high performance concrete for precast/prestressed concrete industry. Case Studies in Construction Materials, 2019, Vol. 11 https://doi.org/10.1016/j.cscm.2019.e00290
4. Akhnoukh, A.K. Overview of nanotechnology applications in construction industry in the United States. Journal of Micro and Nano-systems, 2013, Vol. 5, No. 2, pp. 147-153
5. Akhnoukh, A.K. The use of micro and nano-sized particles in increasing concrete durability. Particulate Science and Technology, 2019, Vol. 38, No. 5, pp. 529-534 https://doi.org/10.1080/02726351.2018.1467988
6. Ontiveros-Perez, S.P., Miguel, L.F.F., and Riera, J.D. Reliability-based optimum design of passive friction dampers in buildings in seismic regions. Engineering Structures, 2019, Vol. 190, 2019, pp. 276-284 https://doi.org/10.1016/j.engstruct.2019.04.021
7. Armali, M., Damerji, H., Hallal, J, and Fakih, M. Effectiveness of friction dampers on the seismic behavior of high rise building vs. shear wall system. Engineering Reports, 2019, Vol. 1, No. 5, https://doi.org/10.1002/eng2.12075
8. Pall, A., and Pall, R.T. Performance-based design using pall friction dampers – an economical design solution. Proceedings of the 13th World Conference on Earthquake Engineering, Vancouver, B.C., Canada, 2004
9. Malhotra, A., Roy, T., and Matsagar, V. Effectiveness of friction dampers in seismic and wind response control of connected adjacent steel buildings. Shock and Vibration, 2020 https://doi.org/10.1155/2020/8304359
10. Elias, S., Rupakhety, R., and Olafsson, S. Tuned mass dampers for response reduction of a reinforced concrete chimney under near-fault pulse-like ground motions. Front. Built. Environ., 2020, Vol. 6 https://doi.org/10.3389/fbuil.2020.00092
11. Teplyshev, V., Mylnik, A., Pushkareva, M., Agakhanov, M., and Burova, O. Application of tuned mass dampers in high-rise construction. Proceedings of the E3S Web of Conferences, 2018 https://doi.org/10.1051/e3sconf/20183302016
12. Amjadian, M. A study on the use of an energy-regenerative tuned mass damper for vibration control and monitoring of base-isolated buildings. Proceedings of the SPIE Smart Structures + Nondestructive Evaluation, Long Beach, California, 2022, https://doi.org/10.1117/12.2610866
13. Infanti, S, Robinson, J., and Smith, R. Viscous dampers for high-rise buildings. Proceedings of the 14th World Conference on Earthquake Engineering, Beijing, China, 2008
14. Del Gobbo, G.M., Blakeborough, A., and Williams, M.S. Improving total-building seismic performance using linear fluid viscous dampers. Bulletin of Earthquake Engineering, 2018, Vol. 16, pp. 4249-4272 https://doi.org/10.1007/s10518-018-0338-4
15. Chen, P., and Wu, X. Investigations on the dynamic response of adjacent buildings connected by viscous dampers. Buildings, 2022, Vol. 12, https://doi.org/10.3390/buildings12091480
16. Kandemir-Mazanoglu, E.C., and Mazanoglu, K. An optimization study for viscous dampers between adjacent buildings. Mechanical Systems and Signal Processing, 2017, Vol. 89, pp. 88-96. https://doi.org/10.1016/j.ymssp.2016.06.001
17. Occhiuzzi, A., Spizzuoco, M., and Serino, G. Experimental analysis of magnetorheological dampers for structural control. Smart Materials and Structures, 2003, Vol. 12, No. 5 DOI 10.1088/0964-1726/12/5/306
18. Zhu, X., Jing, X., and Cheng, Li. Magnetorheological fluid dampers: a review on structure design and analysis. Journal of Intelligent Material Systems and Structures, 2012 DOI: 10.1177/1045389X12436735

19. Guo, Y.Q., Xie, W.H., and Jing, X. Study on structures incorporated with MR damping material based on PSO algorith. Front. Mater., 2019, Vol. 6, No. 73 https://doi.org/10.3389/fmats.2019.00037
20. Abdul-Aziz, M., Mohtasim, S.M., and Ahammed, R. State-of-the-art recent developments of large magnetorheological (MR) dampers: a review, Korea-Austria Rheological Journal, 2022, Vol. 34, pp. 105-136 https://doi.org/10.1007/s13367-022-00021-2
21. Baheti, A.S., and Matsagar, V.A. Wind and seismic response control of dynamic similar adjacent buildings connected using magneto-rheological dampers. Infrastructures, 2022, Vol. 7, No. 12, https://doi.org/10.3390/infrastructures7120167
22. Amezquita-Sanchez, J.P., Valtierra-Rodriguez, M., Aldwaik, M., and Adeli, H. Neurocomputing in civil infrastructure. Sci Iran, 2016, Vol. 23, No. 6, pp. 2417-2428
23. Salehi, H., Burguen, R., Chakrabartty, S., Lajnef, N., and Alavi, A.H. A comprehensive review of self-powered sensors in civil infrastructure: state-of-the-art and future research trends. Eng. Struct. 234:111963
24. Muthalif, A.G., Kasemi, H.G., Nordin, N.D., Rashid, M., and Razali, M.K.M. Semi-active vibration control using experimental model of magneto-rheological damper. Smart Structures and Systems, 2017, Vol. 20, No. 1, pp. 85-97 DOI: 10.12989/sss.2017.20.1.085
25. Maciejewski, I., Krzyzynski, T., Pecolt, S., and Chamera, S. Semi-active vibration control of horizontal seat suspension by using magneto-rheological damper. Journal of Theoretical and Applied Mechanics, 2019, Vol. 57, No. 2, pp. 411-420 DOI: https://doi.org/10.15632/jtam-pl/104593
26. Bai, X.X., Jiang, P., Qian Integrated semi-active seat suspension for both longitudinal and vertical isolation. Journal of Intelligent Material Systems and Structures, Vol. 28, No. 8 https://doi.org/10.1177/1045389X1666617
27. Dantas, C., Gabriel, F., and da Costa Neto, R., "Influence of the distances between the axles in the vertical dynamics of a military vehicle equipped with magnetorheological dampers. SAE Technical Paper 2018-36-0232, 2018, https://doi.org/10.4271/2018-36-0232
28. Ashianti, M., Hashemabadi, S., and Ghaffari, A. A review on the magnetorheological fluid preparation and stabilization. J. Magn. Magn. Mater., 2015, Vol. 374, pp. 716-730 https://doi.org/10.1016/j.jmmm.2014.09.020
29. Kumar, J.S., Paul, P.S., Raghunathan, G., and Alex, D.G. A review of challenges and solutions in the preparation and use of magnetorheological fluids. International Journal of Mechanical and Material Engineering, 2019, Vol. 14, No. 13, https://doi.org/10.1186/s40712-019-0109-2
30. Khedkar, Y.M., Bhat, S., an Adarsha, H. A review of magneto-rheological fluid damper technology and its applications. International Review of Mechanical Engineering, 2019, Vol. 13, No. 4, pp. 256-264
31. X. Wang, D.H., and Liao, W.H. Semiactive controllers for magnetorheological fluid dampers. Journal of Intelligent Material Systems and Structures, 2016, Vol. 16 https://doi.org/10.1177/1045389X05055281
32. Yao, G., Yap, F., Chen, G., Li, W., and Yeo, S. MR damper and its application for semi-active control of vehicle suspension system. Mechatronics, 2002, Vol. 12, No. 7, pp. 963-973
33. Yang, G., Spencer, B., Carlson, J., and Sain, M. Large-scale MR fluid dampers: modeling and dynamic performance considerations. Engineering Structures, 2002, Vol. 24, No. 3, pp. 309-323 https://doi.org/10.1016/S0141-0296(01)00097-9
34. Yang, G., Spencer, B.F., Jung, H.J., and Carlson, D. Dynamic modeling of large-scale magnetorheological damper systems for civil engineering applications. Journal of Engineering Mechanics, 2004, Vol. 130, No. 9, pp. 1107-1114 DOI: 10.1061/~ASCE!0733-9399~2004!130:9~1107!
35. Fujitani, H., Sodeyama, H., Tomura, T., Hiwatashi, T., Shiozaki, Y., Hata, K., Sunakoda, K., Morishita, S., and Soda, S. Development of 400kN magnetorheological damper for a real base-isolated building. 2003, pp. 265-276
36. Xu, Z.D., Sha, L.F., Zhang, X.C., and Ye, H.H. Design, performance test and analysis on magnetorheological damper for earthquake mitigation. Structural Control and Health Monitoring, 2013, Vol. 20, No. 6, pp. 956-970 **https://doi.org/10.1002/stc.1509**
37. Jansen, L.M., and Dyke, S.J. Semiactive control strategies for MR. dampers: comparative study. Journal of Engineering Mechanics, 2000, Vol. 126, No. 8, pp. 795-803
38. Bhardwaj, M.K., and Datta, T.K. Semiactive fuzzy control of the seismic response of buildings frame. Journal of Structural Engineering, 2006, Vol. 132, No. 5, pp. 791-799
39. Bitaraf, M, Ozbulut, O.E., Hurlebaus, S., and Barroso, L. Application of semi-active control strategies for seismic protection of buildings with MR Dampers. Engineering Structures, 2010, Vol. 32, No. 10, pp. 3040-3047
40. Aly, A.M. Vibration control of buildings using magnetorheological damper: A new control algorithm. Journal of Engineering (United Kingdom), 2013, Vol. 2013
41. Bozorgvar, M., and Zahari, S.M. Semi active seismic control of buildings using MR damper and adaptive neural-fuzzy intelligent controller optimized with genetic algorithm. JVC/Journal of Vibration and Control, 2019, Vol. 25, No. 2, pp. 273-285 https://doi.org/10.1177/107754631877450
42. Bathaei, A., Zahari, S.M., and Ramezani, M. Semi-active seismic control of an 11-DOF building model with TMD+MR damper using type-1 and -2 fuzzy algorithms. JVC/Journal of Vibration and Control, 2018, Vol. 24, No. 13, pp. 2938-2953
43. Bagherkhani, A., and Baghlani, A. Reliability assessment of MR fluid dampers in passive and semi-active seismic control of structures. Probabilistic Engineering Mechanics, 2021, Vol. 63
44. Fakhry, A.A., Torky, A.A., and Rashed, Y.F. Optimized seismic response control of coupled FEM-BEM high-rise structural models using magnetorheological dampers. Journal of Earthquake Engineering, 2021, Vol. 11, pp. 1-28
45. Ohtori, Y., Christenson, R.E., Asce, A.M., Spencer, B.F., Asce, M., and Dyke, S.J. Benchmark control problems for seismically excited nonlinear buildings. ASCE Journal of Engineering Mechanics, 2004, Vol. 130, pp 366-385

46. Hasan, A., Torky, A., and Rashed, Y. Geometrically accurate structural analysis models in BIM-centered software. Automation in Construction, Vol. 104, 2019
47. Bonyadi, M.R., and Michalewicz, Z. Particle swarm optimization for single objective continuous space problems: a review Evolutionary Computation, 2017, Vol. 25, no. 1, pp. 1-54
48. Spencer, B.F., Dyke, S.J., Sain, M.K., and Carlson, J.D. Phenomenological model for magnetorheological dampers. Journal of Engineering Mechanics, 1997, vol. 123, no. 3, pp. 230-238
49. Jung, H.J., Spencer, B.F., and Lee, I.W. Control of seismically excited cable-stayed bridge employing magnetorheological fluid dampers. Journal of Structural Engineering, 2003, vol. 129, no. 7, pp. 873-883

Appendix A: State Space representation and LQG

The equation of motion of a multi degree of freedom system can presented in matrix format according to the Eqn. 1 as presented next:

$$\boldsymbol{M}\ddot{U} + \boldsymbol{C}\dot{U} + \boldsymbol{K}U = \Gamma f - \boldsymbol{M}\Lambda\ddot{x}_g \quad (1)$$

Where $\boldsymbol{M}$ is the mass matrix and $\boldsymbol{C}$ is the damping matrix and $\boldsymbol{K}$ is the stiffness matrix for the system. $\ddot{U}$, $\dot{U}$, and U are the acceleration, velocity, and displacement vectors for the system degrees of freedom. The term Γ is a vector donate the locations and weights of an applied force vector f. The $\ddot{x}_g$ is the applied ground excitation and vector Λ is a vector represents the ground excitation directional force distribution.

The previous equation can be represented in state-space formulation presented as:

$x = \begin{bmatrix} U \\ \dot{U} \end{bmatrix}$ is called the state vector and the change in state is presented as $\dot{x} = \begin{bmatrix} \dot{U} \\ \ddot{U} \end{bmatrix}$, rearranging 1, $\ddot{U}$ can be presented in the following format.

$$\ddot{U} = \boldsymbol{M}^{-1}(-\boldsymbol{C}\dot{U} - \boldsymbol{K}U + \Gamma f - \boldsymbol{M}\Lambda\ddot{x}_g) \quad (2)$$

$$\ddot{U} = [-\boldsymbol{K}\boldsymbol{M}^{-1} \quad -\boldsymbol{C}\boldsymbol{M}^{-1}]\begin{bmatrix} U \\ \dot{U} \end{bmatrix} + \Gamma\boldsymbol{M}^{-1}f - \Lambda\ddot{x}_g \quad (3)$$

Then State vector and system response y are presented in the following equation

$$\dot{x} = Ax + Bf + E\ddot{x}_g \quad (4)$$
$$y = Cx + Df + F\ddot{x}_g$$

Where,

$$A = \begin{bmatrix} 0 & I \\ -\boldsymbol{K}\boldsymbol{M}^{-1} & -\boldsymbol{C}\boldsymbol{M}^{-1} \end{bmatrix}, \quad B = \begin{bmatrix} 0 \\ \Gamma\boldsymbol{M}^{-1} \end{bmatrix} \text{ and } E = \begin{bmatrix} 0 \\ -\Lambda \end{bmatrix}$$

$$C = [-\boldsymbol{K}\boldsymbol{M}^{-1} \quad -\boldsymbol{C}\boldsymbol{M}^{-1}], \quad D = [\Gamma\boldsymbol{M}^{-1}] \text{ and } F = [-\Lambda] \quad (5)$$

The control implemented applies semi active control strategy, LQG is used. A combination of a Linear Quadratic Regulator (LQR) and Linear Quadratic Estimator (LQE) using Kalman filter for optimal state estimation. The following cost function is to be minimized

$$J = \lim_{t\to\infty} \frac{1}{t}\left[\int_0^t \{Cx + Df)^T \boldsymbol{Q}(Cx + Df) + f^T \boldsymbol{R} f\} dt\right] \quad (6)$$

Where **R** and **Q** donate weighting matrices and the target of PSO ranges.

Appendix B: Damper Model

The dynamic model used for the numerical analysis for the MR-Damper is the model proposed by Spencer, this phenomenological model is based on the Boc-Wen hysteresis model [48], they presented a prototype MR-Damper with maximum produced force equal to 1000N, the dynamic factors effecting the behavior of the damper are presented in figure 8, where the Bouc-Wen model and MR fluid stiffness k_o and damping c_o are between displacement x and y, while

Preprints (www.preprints.org) | NOT PEER-REVIEWED | Posted: 28 February 2023 doi:10.20944/preprints202302.0518.v1

the additional dashpot c_1 and spring k_1 represent the force roll-off behavior at low velocities and the accumulator unit stiffness, respectively. Force in this damper is obtained through a set of equations presented by Spencer :

$$F = c_1\dot{y} + k_1(x - x_o) \quad (1)$$

Considering equivalent forces at the upper part of the damper

$$c_1\dot{y} = \alpha z + k_o(x - y) + c_o(\dot{x} - \dot{y}) \quad (2)$$

where z is the evolutionary parameter governed by:

$$\dot{z} = -\gamma|\dot{x}|z|z|^{n-1} - \beta\dot{x}|z|^n + A\dot{x} \quad (3)$$

And α is the pre-yield to post-yield ratio, n, γ, β, and A are the parameters that control the hysteresis behavior and are obtained through experimental means {48]

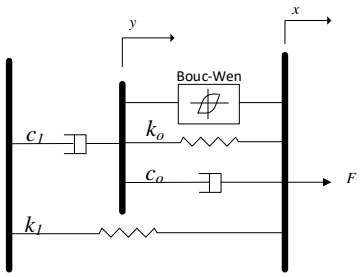

Figure 29. Modified Bouc-Wen Model proposed by Spencer [48]

A Large MR-damper Modified Bouc-Wen parameters are presented by Jung of 100kN capacity [49] obtained by scaling a 20kN MR-damper 5 times for force and 2.5 times for stroke of the device. The parameters for the used MR-Damper in this study are presented in table 3:

Table 3: The Large MR-Damper parameters obtained from Jung [49]

Parameter	Value
α_a	46.2 kN/m
α_b	41.2 kN/m /V
c_{0a}	110.0 kN s/m
c_{0b}	114.3 kN s/m /V
c_{1a}	8359.2 kN s/m
c_{1b}	7482.9 kN s/m /V
η	100 s−1
$k0$	0.002 kN/m
$k1$	0.0097 kN/m
γ	164.0 m−2
β	164.0 m−2
A	1107.2
n	2

In this model, three parameters depend on the current driver u:

$$\alpha(u) = \alpha_a + \alpha_b u\,,\ c_o(u) = c_{oa} + c_{ob}u\,, \text{and } c_1(u) = c_{1a} + c_{1b}u \quad (4)$$

Preprints (www.preprints.org) | NOT PEER-REVIEWED | Posted: 28 February 2023 doi:10.20944/preprints202302.0518.v1

the first order filter $\dot{u} = -\eta(u - v)$ where v is the applied voltage to the current driver donates the current involvement in the MR fluid to reach rheological equilibrium [48]